6604 *Inorg. Chem.* **2009**, *48*, 6604–6614
DOI: 10.1021/ic900571v

Inorganic Chemistry
Article

Novel Bispidine Ligands and Their First-Row Transition Metal Complexes: Trigonal Bipyramidal and Trigonal Prismatic Geometries

Peter Comba,* Christina Haaf, and Hubert Wadepohl

Universität Heidelberg, Anorganisch-Chemisches Institut, INF 270, D-69120 Heidelberg, Germany

Received March 24, 2009

Four very rigid second generation bispidine-based ligands (bispidine = 3,7-diazabicyclo[3.3.1]nonane; tetra-, penta- and hexadentate; exclusively tertiary amine donors except for one of the pentadentate ligands, where one of the donors is a pyridyl group) and their Co^{II}, Ni^{II}, Cu^{II}, and Zn^{II} complexes are reported. The experimentally determined X-ray crystal structures and computational data, based on empirical force field (MM) and approximate density functional theory (DFT) calculations, indicate that these new ligands, which are based on a modular system and therefore allow for a wide range of donor sets and coordination geometries, have rather large cavities (i.e., lead to a preference for +II over +III oxidation states and induce relatively low ligand fields), enforce trigonal geometries (pentacoordinate systems: preference for trigonal bipyramidal, hexacoordinate complexes: preference for trigonal prismatic), and lead, especially for Cu^{II}, to very high complex stabilities.

Introduction

Bispidine derivatives (3,7-diazabicyclo[3.3.1]nonane) were first reported by Mannich.[1] The first bispidine metal complexes were prepared and characterized in the 1950s and 1960s,[2,3] and the development of the transition metal coordination chemistry of the tetra-, penta- and hexadentate first generation bispidine ligands (see L^1 in Chart 1 as an example of a tetradentate ligand) started around 10 years ago.[4,5] Ligands such as L^1 are extremely rigid and enforce a *cis*-octahedral (or square-pyramidal) coordination geometry to transition metal ions,[6,7] and the specific distortions lead to interesting properties such as unusual isomerism,[7−10] efficient models for oxygen-activating copper and iron enzymes,[11−14] technical[15] and medicinal applications.[16]

The majority of the first generation of bispidine ligands has at least two aromatic nitrogen donors which are *trans*-disposed in their complexes and enforce the specific geometries described above.[5] While decisive for a variety of interesting properties, this limits the accessible coordination geometries and the ensuing electronic structures and applications. Also, there is a limited number of available heteroaromatic aldehydes and amines, which, in the Mannich condensation steps yield the desired products, and these are relatively expensive, specifically in view of technical applications. Recently, we have shown how to overcome both limitations: donors in addition to the two tertiary amines N3 and N7 may be introduced exclusively via the amine component, if this bears more than one donor, such as the amine component 1,4,6-trimethyl-1,4-diazaepan-6-amine,[17] used for the synthesis of L^2 in Chart 1.[21,22]

*To whom correspondence should be addressed. E-mail: peter.comba@aci.uni-heidelberg.de. Fax: +49-6221-546617.

(1) Mannich, C.; Mohs, P. *Chem. Ber.* **1930**, *B63*, 608.
(2) Stetter, H.; Merten, R. *Chem. Ber.* **1957**, *90*, 868.
(3) Haller, R. *Arch. Pharm.* **1969**, *302*, 113.
(4) Comba, P.; Nuber, B.; Ramlow, A. *J. Chem. Soc., Dalton Trans.* **1997**, 347.
(5) Comba, P.; Kerscher, M.; Schiek, W. *Prog. Inorg. Chem.* **2008**, *55*, 613.
(6) Comba, P.; Lienke, A. *Inorg. Chem.* **2001**, *40*, 5206.
(7) Comba, P.; Kerscher, M.; Merz, M.; Muller, V.; Pritzkow, H.; Remenyi, R.; Schiek, W.; Xiong, Y. *Chem.—Eur. J.* **2002**, *8*, 5750.
(8) Comba, P.; Kerscher, M.; Lawrance, G. A.; Martin, B.; Wadepohl, H.; Wunderlich, S. *Angew. Chem., Int. Ed.* **2008**, *47*, 4743.
(9) Bentz, A.; Comba, P.; Deeth, R. J.; Kerscher, M.; Pritzkow, H.; Seibold, B.; Wadepohl, H. *Inorg. Chem.* **2008**, *47*, 9518.
(10) Born, K.; Comba, P.; Kerscher, M.; Rohwer, H. *Dalton Trans.* **2009**, 362.
(11) Börzel, H.; Comba, P.; Pritzkow, H. *J. Chem. Soc., Chem. Commun.* **2001**, 97.
(12) Börzel, H.; Comba, P.; Hagen, K. S.; Kerscher, M.; Pritzkow, H.; Schatz, M.; Schindler, S.; Walter, O. *Inorg. Chem.* **2002**, *41*, 5440.
(13) (a) Bukowski, M. R.; Comba, P.; Limberg, C.; Merz, M.; Que, L.Jr.; Wistuba, T. *Angew. Chem., Int. Ed.* **2004**, *43*, 1283.
(14) Bautz, J.; Comba, P.; Lopez , C.; Menzel, M.; Rajaraman, G. *Angew. Chem., Int. Ed.* **2007**, *46*, 8067.
(15) Börzel, H.; Comba, P.; Hage, R.; Kerscher, M.; Lienke, A.; Merz, M. *Ligand and complex for catalytically bleaching a substrate*. Patent WO 0248301 A1, June 20, 2002; U.S. Patent 2002/014900, October 17, **2002**.
(16) Juran, S.; Walther, M.; Stephan, H.; Bergmann, R.; Steinbach, J.; Kraus, W.; Emmerling, F.; Comba, P. *Bioconjugate Chem.* **2009**, *20*, 347.
(17) This heterocyclic, amine-substituted building block has been described before.[18−20]
(18) Appel, A. C. M.; Hage, R.; Russell, S. W.; Tetard, D. Unilever, WO-A 0185717 **2000** (*Chem. Abstr.* **2001** *135*, 359431).
(19) Peralta, R. A.; Neves, A.; Borloluzzi, A. J.; Casellato, A.; dos Anjos, A.; Greatti, A.; Xavier, F. R.; Szpoganicz, B. *Inorg. Chem.* **2005**, *44*, 7690.
(20) Aime, S.; Calabi, L.; Cavallotti, C.; Gianolio, E.; Giovenuzana, G. B.; Losi, P.; Maiocchi, A.; Palmisanno, G.; Sisti, M. *Inorg. Chem.* **2004**, *43*, 7588.
(21) P. Comba, C. Haaf, M. Kerscher, A. Lienke, *Bispidinliganden und ihre Metallkomplexe*, PCT/EP 2008/004506 DE 10 2007 033 020, **2009**
(22) P. Comba, C. Haaf, A. Lienke, A. Muruganantham, H. Wadepohl, submitted **2009**.

 Published on Web 05/20/2009

Chart 1

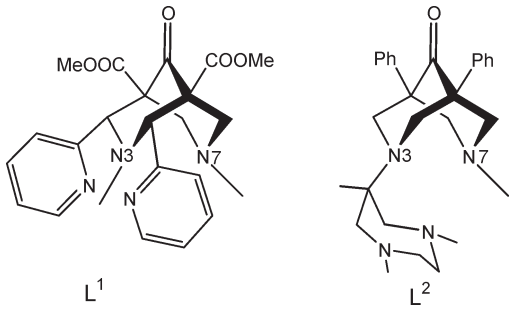

The resulting second generation bispidine ligands combine the rigidity of the adamantane-derived backbone with that of azamacrocyclic ligands. More importantly, this ligand architecture makes new coordination geometries accessible: molecular models show that the tetradentate ligand L^2 with four tertiary amine donors (see Chart 1) enforces coordination geometries derived from trigonal bipyramidal, and this also is the case for pentadentate derivatives obtained by condensation with a monofunctionalized amine in the second Mannich reaction, such as ethane-1,2-diamine derivatives used for L^3 or picolylamine used for L^4 (see Scheme 1). With hexadentate ligands, bearing two 1,4,6-trimethyl-1,4-diazepan-6-amine subunits (L^5 in Scheme 1), geometries derived from trigonal prismatic are obtained. These predictions are supported by force field and density functional theory (DFT) calculations (see Supporting Information), and are substantiated by the X-ray crystal structures reported in this communication. Obviously, through a variation of the primary amine building block, the synthetic strategy shown in Scheme 1 allows the wide variation of rigid coordination geometries and donor sets, and a number of such ligands are currently prepared in our laboratory. Here, we report the syntheses, structural, and solution properties of the first series of tetra-, penta-, and hexadentate bispidine ligands L^2−L^5 and their trigonal bipyramidal and trigonal prismatic first-row transition metal complexes.

Results and Discussion

Syntheses. The piperidone P (3,5-diphenyl-1-(1,4,6-trimethyl-1,4-diazepan-6-yl)piperidin-4-one; see Scheme 1) is obtained in acceptable yields by the condensation of 1,3-diphenylpropane-2-on with 1,4,6-trimethyl-1,4-diazepan-6-amine and formaldehyde.[21,22] This general building block for a wide range of multidentate bispidine ligands has been used here to prepare the tetradentate ligand L^2 [21,22] and the two pentadentate bispidines L^3 and L^4; the hexadentate ligand L^5 is obtained in a one-step double-Mannich reaction from 1,3-diphenylpropane-2-on, 2 equiv of 1,4,6-trimethyl-1,4-diazepan-6-amine, and 4 equiv of aqueous formaldehyde. The overall yield for all four ligands is between 25% and 60%. Divalent first-row transition metal complexes were obtained by relatively fast complexation from stoichiometric ligand/metal salt mixtures in MeCN or MeOH solutions in 19−70% yield, and single crystals for X-ray diffraction were isolated for a number of the complexes, generally by slow diffusion of diethylether into the reaction mixture solutions of the complexes.

Structural Properties. The structures of the ligands, determined by single crystal X-ray diffraction, are dominated by lone-pair repulsion, which enforces the chair-boat conformation of the bispidine backbone.[5] Also, the diazacycloheptane ring is, as expected, not well preorganized for coordination to a metal ion, see Figure 1 and Table 1.[23] However, the required conformational changes for coordination of these ligands to transition metal centers are expected to be low energy processes, and the corresponding complexes therefore are assumed to be very stable.[5,7,24]

The X-ray crystal structure of the Cu^{II} complex of the tetradentate ligand L^2 has been reported before,[22] and the structures of the corresponding *high-spin* Co^{II} and Zn^{II} complexes are isostructural, that is, distorted trigonal bipyramidal, with an axial MeCN ligand completing the coordination sphere (see Figure 2 and Table 2). This suggests that the distorted trigonal bipyramidal structure is enforced by the rigid bispidine ligand L^2 and, as expected, the DFT- and MM-optimized structures (see Supporting Information for these data) accurately reproduce the observed geometries. It emerges that the predicted structures of complexes without experimentally determined structures (e.g., that of the Ni^{II} complex of L^2) are reliable, and this also is assumed to be so for the distorted trigonal bipyramidal complexes of L^3 and L^4 and the distorted trigonal prismatic complexes of L^5.

The main distortion from trigonal bipyramidal for the tetra- and pentadentate ligand L^2, L^3, and L^4 complexes is a very small N1−M−N2 angle (75−78° instead of the regular 120°) and correspondingly large N1−M−N7 and N2−M−N7 angles of approximately of 140°.[25] The rigid six-membered chelate rings involving the bispidine donors N3 and N7 lead, depending on the metal-donor distances, to angles involving the metal center of close to 90°.[5,7] Combined with the steric effects of the substituents at N1 and N2, this leads to a ligand fragment which enforces a trigonal pyramidal structure with N3 as the apical ligand. The amount of distortion within the "trigonal plane", involving M, N1, N2, and N7, may be adjusted by the size of the diazamacrocyclic ring fragment, specifically by the bridge between the two donors N1 and N2. This is an important design principle for these second generation bispidine ligands and has already proven to be a useful concept in the copper-catalyzed aziridination reaction.[22]

The second significant mode of distortion for the pentacoordinate complexes involves the angle of the metal center with the two axial donors N3 and N4, and this is especially pronounced for the pentadentate ligand systems L^3 and L^4. That is, the size and shape of the chelate ring involving N7 and N4 may be used to enforce a particular distortion to the metal center: with the tetradentate ligand L^2 and a monodentate axial donor N4, the N3−M−N4 axis generally is close to 180°, and with the pentadentate ligands L^3 and L^4 significant distortions to

(23) Bocian, D. F.; Pickett, H. M.; Rounds, T. C.; Strauss, H. L. *J. Am. Chem. Soc.* **1975**, *97*, 687.
(24) Born, K.; Comba, P.; Ferrari, R.; Kuwata, S.; Lawrance, G. A.; Wadepohl, H. *Inorg. Chem.* **2007**, *46*, 458.
(25) Note that the large asymmetry with respect to these two angles in some of the complexes is due to a distortion towards square pyramidal. This depends on the size of the metal ion and, to some extent, also on the electronic properties of the metal center, and is reasonably well reproduced by the computational data (see Supporting Information).

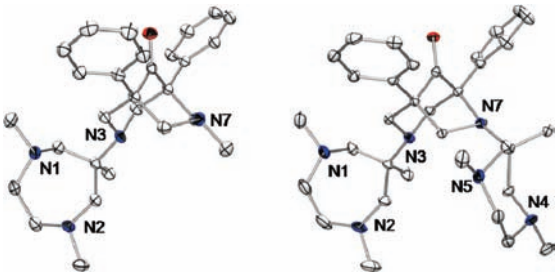

Figure 1. Ortep plots of the metal-free bispidone ligands L^2 and L^5; hydrogen atoms are omitted for clarity.

Table 1. Selected Experimental Structural Data of the Metal-Free Ligands L^2 and L^5

	L^2	L^5
	Distances [Å]	
N3−N7	3.460(2)	3.493(2)
N1−N2	2.961(2)	2.990(2)
N4−N5		3.027(2)
	Angles [deg]	
N3−C=O−N7	79.05(5)	80.59(6)
	Torsional Angles [deg]	
C=O−N3−C_{tert}−C_{Me}	107.60	111.28
C=O−N7−C_{tert}−C_{Me}		−52.24

Scheme 1. Synthesis of the Second Generation Bispidine Ligands and Their Complexes

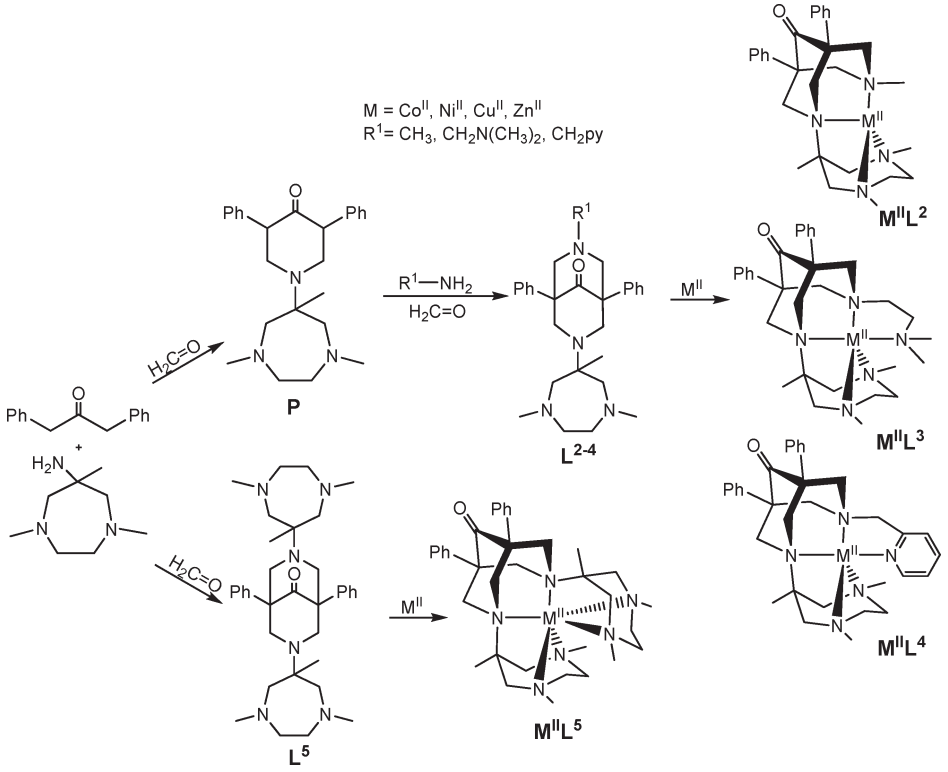

around 160° (dependent on the metal-donor distances) are observed. Clearly, this significantly influences the ligand field and thermodynamic properties and is a second important design possibility for this second generation bispidine ligands (see solution properties below).

Following the structural discussion above, the two bispidine-based amine donors N3 and N7 of the hexadentate ligand L^5 each are part of a "trigonal plane" which also involves the metal center (M, N3, N4, N5 and M, N7, N1, N2), and, because of the rigidity of the bispidine backbone, the resulting coordination geometries are expected to be distorted trigonal prismatic. This also follows from model calculations (see Supporting Information) and suggests again that the observed distorted trigonal prismatic structures (see Figure 2 and Table 2) are enforced by the ligand. Arguments based on ligand field theory and intraligand repulsion effects[26,27] suggest that this may lead to subtle effects with respect to the complex stabilities, for example, related to Irving−Williams-series-type behavior[28] or unusual effects with respect to the denticity of the ligands,[24] see also below.

Interestingly, the Cu^{II}−N distances to the amines within each macrocyclic subunit of the $Cu^{II}L^5$ complex are very asymmetric (Cu−N1 vs Cu−N2 and Cu−N4 vs Cu−N5, respectively, see Figure 2 and Table 2). To some extent, this asymmetry is also observed in the structure of the $Co^{II}L^5$ and $Ni^{II}L^5$ complexes, and it is reproduced or predicted in the MM and DFT calculations of the Co^{II}, Ni^{II}, Cu^{II}, and Zn^{II} complexes (see Supporting Information and Table 2, respectively[31]). Interestingly, the experimentally determined $Ni^{II}L^5$ structure is highly distorted (see Table 2 and Figure 2) with a very long M−N1 bond,

(26) Comba, P.; Engelhardt, L. M.; Harrowfield, J. M.; Horn, E.; Sargeson, A. M.; Snow, M. R.; White, A. H. *Inorg. Chem.* **1985**, *24*, 2325.
(27) Comba, P. *Inorg. Chem.* **1989**, *28*, 426.

(28) This is supported by the observed stability constants, which do not follow the typical Irving-Williams series behavior[29,30] (see section on solution properties), i.e., there is no size-match selectivity.[24]
(29) Irving, H.; Williams, R. J. P. *Nature* **1948**, *162*, 746.
(30) Irving, H.; Williams, R. J. P. *J. Chem. Soc.* **1953**, 3192.
(31) For the MM calculations of the Cu^{II} complex an approach with two different parameter sets for the axial and in-plane bonds was used.[32]
(32) Stratemeier, H.; Hitchman, M. A.; Comba, P.; Bernhardt, P. V.; Riley, M. J. *Inorg. Chem.* **1991**, *30*, 4088.

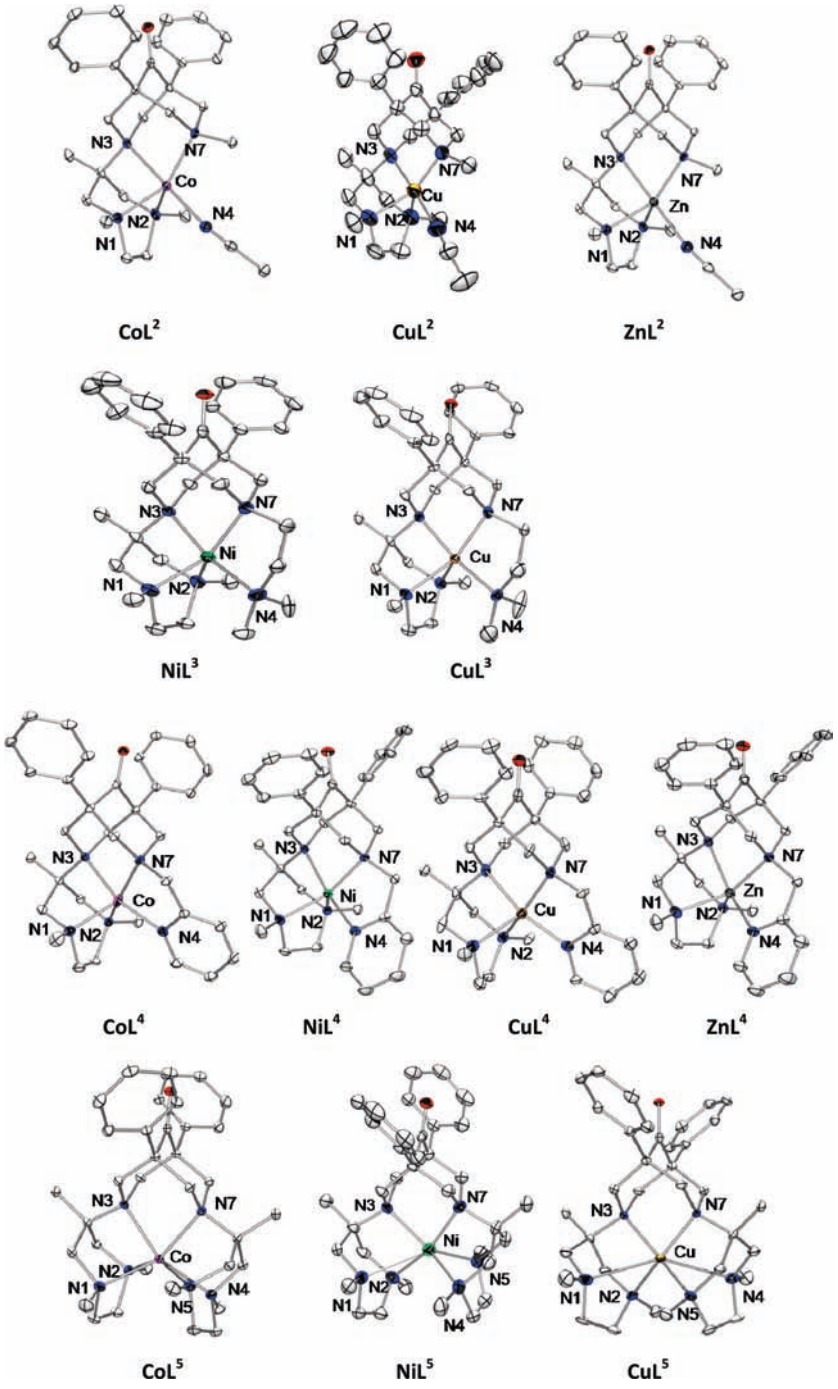

Figure 2. Ortep plots of the molecular cations of the experimentally determined X-ray structures of $[Co^{II}(L^2)(NCCH_3)](ClO_4)_2$, $[Cu^{II}(L^2)(NCCH_3)](BF_4)_2$,[22] $[Zn^{II}(L^2)(NCCH_3)](ClO_4)_2$, $[Ni^{II}(L^3)](ClO_4)_2$, $[Cu^{II}(L^3)](BF_4)_2$, $[Co^{II}(L^4)](ClO_4)_2$, $[Ni^{II}(L^4)](ClO_4)_2$, $[Cu^{II}(L^4)](BF_4)_2$, $[Zn^{II}(L^4)](ClO_4)_2$, $[Co^{II}(L^5)](BF_4)_2$, $[Ni^{II}(L^5)](ClO_4)_2$, $[Cu^{II}(L^5)](BF_4)_2$; hydrogen atoms, counterions, and solvent molecules omitted for clarity.

a significantly elongated but much shorter M−N5 bond, and "normal" M−N1 and M−N2 distances (the macrocycle conformations indicate that M−N1 may be interpreted as a "bond"). The elongation along M−N1/M−N5 is reproduced in the DFT calculations but the asymmetry is not, and the high degree of distortion is not reproduced in the MM structure optimization. We interpret these observations as follows: (i) The elongation of a pair of M−N bonds to macrocyclic tertiary amines (pseudo-trans with respect to the distorted trigonal prismatic−trigonal antiprismatic geometry) is supported by the ligand architecture (enforced small N1−M−N2 and N4−M−N5 angles). (ii) Ligand field effects lead to a preference for octahedral over trigonal prismatic, and this is especially pronounced for high-spin d^3 and d^8 as well as for low-spin d^6, that is, in the series studied here for Ni^{II}.[26,27] (iii) These effects are not accounted for in our presently used MM approach. Also, the harmonic metal-donor bonding potentials do not allow for significant elongations. These deficiencies of our Momec force field are currently under review. The assumption that the experimentally observed strong Jahn−Teller elongation might be supported by the ligand structure, leading to a highly complementary ligand for Cu^{II}, was studied with

Table 2. Selected Experimental (X-ray) and Computed (DFT, Italicized) Structural Parameters of the $M^{II}L^2$, $M^{II}L^3$, $M^{II}L^4$ and $M^{II}L^5$ complexes (M = Co, Ni, Cu, Zn)

distances [Å]	$[Co(L^2)(NCMe)]^{2+}$	$[Ni(L^2)X]^{2+}$ [a]	$[Cu(L^2)^{22}(NCMe)]^{2+}$	$[Zn(L^2)(NCMe)]^{2+}$	$[Ni(L^3)]^{2+}$	$[Cu(L^3)]^{2+}$	$[Zn(L^3)]^{2+}$	$[Co(L^4)]^{2+}$	$[Ni(L^4)]^{2+}$	$[Cu(L^4)]^{2+}$	$[Zn(L^4)]^{2+}$	$[Co(L^5)]^{2+}$	$[Ni(L^5)]^{2+}$	$[Cu(L^5)]^{2+}$
M−N3	2.165(2)		1.999(3)	2.1770(15)	2.078(3)	2.032(3)		2.060(2)	2.070(3)	2.030(5)	2.146(2)	2.1790(13)	2.201(6)	2.046(3)
	1.990	*1.982*	*2.008*	*2.022*	*2.083*	*2.029*	*2.157*	*2.148*	*2.067*	*2.008*	*2.141*	*2.190*	*2.148*	*2.046*
M−N7	2.101(2)		2.032(3)	2.0686(14)	2.113(3)	2.072(3)		2.017(2)	2.073(2)	2.016(5)	2.139(2)	2.2031(13)	2.077(6)	2.046(3)
	1.997	*1.998*	*2.069*	*1.982*	*2.143*	*2.071*	*2.151*	*2.135*	*2.106*	*2.054*	*2.153*	*2.190*	*2.160*	*2.046*
M−N1	2.107(2)		2.169(4)	2.1064(16)	2.099(3)	2.176(3)		2.101(2)	2.129(3)	2.175(5)	2.210(2)	2.3104(15)	3.093(6)	2.891
	2.095	*2.061*	*2.223*	*2.079*	*2.129*	*2.335*	*2.214*	*2.243*	*2.195*	*2.156*	*2.262*	*2.378*	*2.460*	*2.988*
M−N2	2.105(2)		2.195(4)	2.0952(16)	2.102(4)	2.274(3)		2.107(2)	2.044(3)	2.177(5)	2.068(2)	2.2899(15)	2.131(6)	2.048(3)
	2.086	*2.080*	*2.224*	*2.080*	*2.176*	*2.237*	*2.149*	*2.131*	*2.085*	2.391	*2.109*	*2.409*	*2.386*	*2.113*
M−N4	2.062(2)		1.969(4)	2.1240(18)	2.123(4)	2.058(3)		2.022(2)	2.042(3)	2.010(5)	2.048(2)	2.2870(12)	2.114(6)	2.890(3)
	2.000		*2.003*		*2.229*	*2.137*	*2.243*	*2.095*	*2.089*	*2.031*	*2.114*	*2.378*	*2.363*	*2.986*
M−N5												2.3562(16)	2.266(6)	2.048(3)
												2.409	*2.398*	*2.113*
Σ(M−N)	10.54		10.36	10.57	10.52	10.61		10.31	10.36	10.41	10.61	13.63	13.88	13.97
$(M-N_{average})$	(2.11)		(2.07)	(2.11)	(2.10)	(2.12)		(2.06)	(2.07)	(2.08)	(2.12)	(2.27)	(2.78)	(2.33)
N3···N7	2.805		2.788	2.820	2.771	2.768		2.735	2.794	2.758	2.822	2.799	2.831	2.819
	2.895	*2.892*	*2.799*	*2.892*	*2.822*	*2.798*	*2.840*	*2.834*	*2.816*	*2.799*	*2.858*	*2.846*	*2.833*	*2.848*
N1···N2 (N4..N5)			2.703	2.691	2.656	2.720		2.648	2.648	2.678	2.713	2.779(2.774)	2.887(2.692)	2.817(2.817)
	2.714	*2.728*		*2.726*	*2.703*	*2.767*	*2.757*	*2.736*	*2.699*	*2.752*	*2.759*	*2.820(2.820)*	*2.830(2.810)*	*2.867(2.866)*

angles [deg]	$Co(L^2)$	$Ni(L^2)$	$Cu(L^2)$	$Zn(L^2)$	$Ni(L^3)$	$Cu(L^3)$	$Zn(L^3)$	$Co(L^4)$	$Ni(L^4)$	$Cu(L^4)$	$Zn(L^4)$	$Co(L^5)$	$Ni(L^5)$	$Cu(L^5)$
N3−M−N4	179.36(5)		176.75(15)	179.68(6)	167.19(13)	170.89(10)		163.04(7)		165.7(2)	157.44(7)	147.53(4)	138.7(2)	157.55(12)
			176.905		*166.545*	*170.938*	*165.257*	*159.439*	*162.450*	*162.940*	*157.783*	*147.068*	*151.031*	*133.970*
N3−M−N7	82.22(5)		87.50(13)	83.22	82.77	84.85(9)		84.27(7)		85.95(19)	82.35(7)	81.08(5)	82.8(2)	87.01(16)
	93.112	*92.493*	*87.952*	*92.493*	*83.769*	*86.027*	*82.469*	*82.857*	*84.876*	*87.078*	*83.440*	*81.069*	*82.249*	*88.223*
N3−M−N1	82.79(5)		86.15(13)	83.94(5)	86.25(13)	85.44(9)		84.51(7)		83.2(2)	84.19(7)	84.24(5)	65.1(2)	87.63(12)
	92.161	*91.887*	*85.230*	*90.903*	*85.004*	*83.694*	*84.095*	*83.587*	*86.492*	*86.300*	*84.504*	*82.453*	76.305	*72.161*
N4−M−N7	97.26(5)		95.64(15)	97.01(6)	84.51(14)	86.07(10)		83.86(7)		84.4(2)	81.65(8)	75.99(4)	85.9(2)	87.63(12)
			95.142		*83.027*	*85.328*	*83.315*	*82.282*	*82.207*	*83.865*	*81.383*	*82.455*	*84.117*	*72.195*
N1−M−N2	79.07(5)		76.56(14)	79.65	78.41(13)	75.41(99		78.62(7)		76.0(2)	78.65(7)	74.33(4)	64.0(2)	
	80.956	*81.898*	*76.091*	*81.898*	*77.779*	*74.461*	*78.367*	*77.394*	*78.151*	*74.279*	*78.186*	72.190	*71.526*	*65.806*
N4−M−N5[b]												73.35(5)	75.8(2)	
												72.188	*72.335*	*65.834*
N1−M−N7[c]	137.69(5)		144.61(14)	137.89(5)	142.63(14)	146.27(10)		125.50(7)		128.8(2)	147.31(7)	142.75(4)	119.6(2)	157.55(12)
	140.089	*138.767*	*141.374*	*138.767*	*133.466*	*143.603*	*141.638*	*147.889*	*153.604*	*136.029*	*146.254*	*147.068*	*127.999*	*133.931*
N2−M−N7[c]	137.69(5)		137.14(14)	138.56(6)	135.57(14)	134.90(10)		153.07(7)		152.6(2)	129.41(7)	130.77(4)	161.6(2)	157.55(12)
	138.132	*130.912*	*141.067*	*139.051*	*145.571*	*138.884*	*135.431*	*129.356*	*125.857*	*147.534*	*132.094*	*130.166*	*151.720*	*155.940*

[a] Computed without coligand. [b] For hexadentate ligands. [c] For pentadentate ligands.

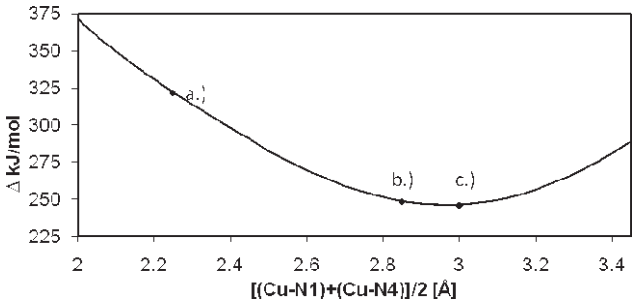

Figure 3. Molecular-mechanics-derived steric energy (no electronic terms included) of $[Cu^{II}L^5]^{2+}$ as a function of the elongation along the N1−Cu−N4 axis (see text for details).

the computational analysis of the cavity size and shape by an established molecular mechanics approach (see Figure 3).[33−35] Point (a) in Figure 3 corresponds to an optimized structure of an electronically innocent metal ion with average bond distances corresponding approximately to Cu^{II} (Cu−N1 = Cu−N4 = 2.23 Å, ΔE_{strain} = 75 kJ/mol). Point (b) corresponds approximately to the bond distances observed in the X-ray structure (Cu−N1 = Cu−N4 = 2.89 Å, ΔE_{strain} = 2 kJ/mol, that is, stabilized by 73 kJ/mol with respect to the "regular structure" above). Point (c) corresponds to the minimum energy structure with respect to the computed curve (Cu−N1 = Cu−N4 = 3.00 Å, ΔE_{strain} = 0 kJ/mol). It follows that the observed significantly elongated $Cu^{II}L^5$ structure is very close to the minimum on the potential energy curve enforced by the ligand and that metal centers which prefer rather undistorted structures are destabilized to some extent, that is, L^5 is highly complementary for the Jahn−Teller active Cu^{II} center. Also, from these calculations, it follows that the second generation hexadentate bispidine ligand L^5 has a rather large cavity size, that is, large metal ions (lower oxidation states) are preferred by the ligand, and this is similar to the first generation bispidine systems.[24,34]

Solution Properties. The electronic spectra of the Co^{II}, Ni^{II}, and Cu^{II} complexes of L^2, L^3, and L^4 are as expected for the distorted trigonal bipyramidal structures observed in the solid, and those of the hexadentate ligand L^5 are qualitatively in agreement with the expected trigonal prismatic chromophores. That is, because of the ligand requirements (see discussion above) the structures of the complexes in solution probably are largely identical to those measured in the crystal.[36] For the Cu^{II} complexes, this is further supported by the frozen solution EPR spectra (see Experimental Section and Supporting Information for the spin Hamiltonian parameters and the observed and simulated spectra). For the trigonal bipyramidal geometries enforced by L^2, L^3, and L^4, d_{z^2} ground states and for the trigonal prismatic geometry due to L^5, a $d_{x^2-y^2}$ ground state are expected. Interestingly, the large distortion in the trigonal plane of the tetra- and pentadentate ligands (Cu^{II},N1,N2,N7; N1−Cu^{II}−N2 ≪ 120°, see above), induces a strong interaction of the N1 and N2 donor groups with the $d_{x^2-y^2}$ orbital and therefore, a $d_{x^2-y^2}$ ground state emerges, as already described for the $[Cu^{II}(L^2)(NCCH_3)]^{2+}$ complex.[22] The increasing distortion along the N3−Cu−N4 pseudotrigonal axis in the L^3- and L^4-based complexes (see structural discussion above) leads to an enhanced distortion toward square pyramidal and itself should enforce a $d_{x^2-y^2}$ ground state in the Cu^{II}-based d^9 systems.

Table 3. Electrochemical Potentials of the Four Cu^{II} Complexes, in MeCN vs $Ag/AgNO_3$; μ = 0.1; in H_2O vs Ag/AgCl; μ = 0.1[a]

complex	2+/1+ (CH_3CN)	2+/1+ (H_2O)
CuL^2	−377ir	−314ir
CuL^3	−484	−368
CuL^4	−474	−295
CuL^5	−440	−287
CuL^{1} [b]	−417	−425
$CuL^{1\prime}$ [c]	−603	−523
$CuL^{1\prime\prime}$ [d]	−489	−413

[a] See Experimental Section for the corresponding $fc^{o/+}$ potentials, measured with this electrode setup. [b] See Chart 1 for the structure of L^1.[5] [c] $L^{1\prime}$ is the N7 α-methylpyridine-substituted pentadentate derivative of L^1.[24] [d] $L^{1\prime\prime}$ is the N3 α-methylpyridine-substituted pentadentate derivative of L^1.[24]

The reduction potentials of the Cu^{II} complexes are assembled in Table 3, where the potentials for the corresponding complexes of L^1 and the two isomeric pentadentate ligands $L^{1\prime}$ and $L^{1\prime\prime}$ appear for comparison. The $Cu^{II/I}$ redox couples reported here are similar to those for the first generation bispidine ligands.[5,24,37] On one hand the new generation of ligands have exclusively amine donors (except for L^4) and this should stabilize the oxidized form of the copper complexes. The variation in geometry on the other hand (trigonal vs *cis*-octahedral) is expected to lead to a destabilization of the Cu^{II} form and limits the shift of the potentials toward more negative values. The couple involving L^2 is irreversible, and this probably is due to a change of geometry during electron transfer with the tetradentate ligand system. As for the first generation bispidine-$Co^{III/II}$ couples, the reduced form of the L^2-, L^3-, L^4-, and L^5-based Co complexes is unusually stable, that is, the corresponding Co^{II} complexes are air-stable (see Experimental Section and Supporting Information). While for the L^1-derived ligand systems, this is primarily due to the larger ligand cavity than preferred by the *low-spin* Co^{III} center, for the L^2-derived second generation bispidine ligands, the enforced trigonal bipyramidal or trigonal prismatic coordination geometries probably are the major reasons for the irreversible and rather high redox potentials.

The results of the potentiometric titrations of the metal-free ligands L^2, L^3, and L^5, and of corresponding ligand−metal salt mixtures in various solvent mixtures are assembled in Table 4. The first protonation of the ligand occurs at a pK_a of about 12 for L^2, 10 for L^3, and 9 for L^5, and this is attributed to the protonation of one of the tertiary amine groups of the bispidine backbone. These nitrogen

(33) Comba, P.; Okon, N.; Remenyi, R. *J. Comput. Chem.* **1999**, *20*, 781.
(34) Bleiholder, C.; Börzel, H.; Comba, P.; Ferrari, R.; Heydt, A.; Kerscher, M.; Kuwata, S.; Laurenczy, G.; Lawrance, G. A.; Lienke, A.; Martin, B.; Merz, M.; Nuber, B.; Pritzkow, H. *Inorg. Chem.* **2005**, *44*, 8145.
(35) The Cu−N1 and Cu−N4 distances were constrained (stepwise elongation by 0.05 Å), and the rest of the structure was fully optimized at each step).
(36) Note that this is a purely qualitative assessment. The results of the potentiometric titrations indicate that the Co^{II} and Ni^{II} complexes are dominated by MLH and MLOH species, and this agrees with the asymmetric coordination mode of L^5, i.e., one of the six donors might be substituted by OH^- or OH_2. Moreover, 7-coordinate $[ML^5OH_2]^{2+}$ structures might also be accessible.
(37) Comba, P.; Merz, M.; Pritzkow, H. *Eur. J. Inorg. Chem.* **2003**, 1711.

Table 4. Protonation Constants (pK_a) and Complex Stabilities ($logK_{ML}$) in Different Aqueous-Dioxane Mixtures (the Values Reported Are Extrapolated for Pure Water[64−67]); μ = 0.1M (KCl) for Protonation Constants, μ = 0.2M ($NaClO_4$) for Complex Stabilities

	L^2	L^3	L^5
	Protonation Constants		
pK_{a1}	5.93(30)	0.54(14)	2.51(6)
pK_{a2}	10.33(12)	7.17(13)	6.21(6)
pK_{a3}	11.84(4)	9.87(6)	8.86(6)
	Complex Stability Constants		
Cu(I) [a]	[c]	12.80	13.28
Cu(II) [b]			
$[CuL]^{2+}$	26.36(19)	21.99(4)	19.48(13)
$[CuLH]^{3+}$	2.97(42)	2.58(43)	1.34(13)
Co(II)			
$[CoL]^{2+}$	8.18(18)	5.48(15)	
$[CoLH]^{3+}$	8.50(17)	8.42(21)	14.24(21)
$[CoLH_2]^{4+}$	4.08(27)	3.10(25)	8.69(20)
$[CoL(OH)]^{+}$	0.92(26)	4.34(2)	2.13(7)
$[CoL(OH)_2]$	11.68(19)	9.91(2)	9.92(4)
Ni(II)			
$[NiL]^{2+}$	8.97(21)	5.52(9)	
$[NiLH]^{3+}$	5.55(47)	6.76(43)	13.67(13)
$[NiLH_2]^{4+}$	4.70(10)	1.59(92)	8.52(37)
$[NiL(OH)]^{+}$	4.39(70)	3.66(3)	1.04(4)
$[NiL(OH)_2]$	3.53(78)	8.01(51)	9.37(13)
$[NiL(OH)_3]^{-}$	10.10(9)		

[a] Calculated from the Cu^{II} stability constant and the redox potential (see Table 4), using the Nernst equation, T = 298 K.[24,68] [b] Formation of $Cu^{II}L$ determined by ligand−ligand competition titrations in the ratio of 1:1:1 (Cu^{II}/L^n/cyclam). [c] Not available because of the irreversible redox potential.

donors are known to be extremely basic since a "bridging" proton between the N3 and N7 sites leads to a release of strain due to the quenched lone-pair-lone-pair repulsion, that is, some of the bispidine ligands are known to exhibit significant proton sponge behavior.[5,24,38−40] The comparatively low basicity of the new generation of ligands in part is due to the stabilization of the chair−boat conformation, as discussed above on the basis of the solid state structural data. Bispidine ligands with smaller N-based substituents generally occur in the chair−chair conformation[5] and have higher first pK_a values. The second pK_a values of the three ligands studied here is as expected about two log units lower, that is, close to the neutral pH range. This and the third pK_a value, which is rather acidic and therefore less accurately determined, are attributed to the protonation of tertiary amine groups of the macrocyclic subunits.

The bispidine backbone has been found before to be well suited for Cu^{II}, [5−7,24] and, based on the structural data (see above), a high degree of complementarity has also been attributed to the tetradentate and pentadentate ligands, enforcing trigonal bipyramidal, and the hexadentate ligand, enforcing a trigonal prismatic coordination geometry. These predictions are largely fulfilled, that is, the Cu^{II} complexes are the most stable of those studied here (see Table 4). More importantly, the L^2-based Cu^{II} complex is by far the most stable in the series, and, in fact, is more stable than other bispidine-Cu^{II} complexes reported before and similar in stability to [Cu(cyclam)]$^{2+}$ (cyclam = 1,4,7,11-tetraazatetradecane; logK = 27.2).[24,41,42] This is, among others, of importance for nuclear medicinal applications, where the first generation bispidine ligands with considerably lower stabilities have been shown to be of interest because of the relatively high complex stability and the fast complex formation kinetics.[16] The lower stability of the pentadentate ligand L^3 Cu^{II} complex compared to that with the tetradentate ligand L^2 is in a general sense counter-intuitive but similar effects have been described with the first generation bispidine ligands,[24] and the decreasing stability is in agreement with the observed distortion along the trigonal axis (see above). The observed lower Cu^{II} complex stability with the hexadentate ligand L^5 in comparison with the tetradentate ligand L^2- and the pentadentate ligand L^3-based complexes is also in line with the observed structural distortions (see above). The still relatively high stability of the distorted trigonal prismatic complex with L^5, which is higher in fact than the stabilities of all first-generation bispidine-Cu^{II} complexes described before,[24] is believed to be due to the ligand enforced elongation of the N1−Cu−N4 axis (see above and Table 2 and Figure 3). The Co^{II} and Ni^{II} complexes of L^5 are considerably less stable; the fact that these systems are dominated by MLH and MLH_{-1} species indicates that the ligand tries to avoid hexacoordination, and this directly follows from the ligand-enforced elongation of the N1−M−N4 axis (see Figures 2 and 3, see also discussion of the corresponding Ni^{II} structure above).

Conclusion

Four new bispidine ligands with four, five or six tertiary amine donors, which enforce trigonal bipyramidal or trigonal prismatic coordination geometries to metal ions, are reported. The combined rigidity of the bispidine backbone[5] and of macrocyclic ligands[43,44] leads to highly predictable structures and the ensuing molecular properties.[45] The modular structure of these new ligands enables the enforcement of a wide range of structural motifs with widely variable donor groups. The Co^{II}, Ni^{II}, Cu^{II}, and Zn^{II} complexes of the four new ligands described here indicate that the structures are generally as predicted with simple force field or with DFT methods, and the stabilities and electronic properties follow qualitatively the expectations based on the ligand-enforced coordination geometries. It emerges that this second generation of bispidine ligands, while slightly less rigid than the L^1-based first generation bispidines (see Chart 1), offers the advantages of a much wider range of accessible coordination geometries and donor sets.

Experimental Section

Materials and Measurements. The syntheses of L^2 and $[Cu^{II}(L^2)](BF_4)_2 \cdot CH_3CN$ have been described elsewhere.[22] Chemicals (Aldrich, Fluka) were used without further purification if not otherwise stated.

(38) (a) Comba, P.; Pritzkow, H.; Schiek, W. *Angew. Chem.* **2001**, *113*, 2556. *Angew. Chem., Int. Ed.*, **2001**, *40*, 2465.
(39) Hosken, G. D.; Hancock, R. D. *J. Chem. Soc., Chem. Commun.* **1994**, 1363.
(40) Hosken, G. D.; Allan, C. C.; Boeyens, J. C. A.; Hancock, R. D. *J. Chem. Soc., Dalton Trans.* **1995**, 3705.
(41) Parker, D. *Chem. Soc. Rev.* **1990**, 271.
(42) Motekaitis, R. J.; Rogers, B. E.; Reichert, D. E.; Martell, A. E.; Welch, M. J. *Inorg. Chem.* **1996**, *35*, 3821.
(43) Lindoy, L. F. *The chemistry of macrocyclic ligand complexes*; Cambridge University Press: Cambridge, **1989**.
(44) Comba, P., Martin, B. In *Macrocyclic Chemistry, Current Trends and Future Perspectives*; Gloe, K., Ed.; Springer: Heidelberg, **2005**; p 303.
(45) Comba, P.; Kerscher, M. *Coord. Chem. Rev.* **2009**, *253*, 564.

NMR spectra were recorded at 200.13 MHz (^{1}H) and 50.33 MHz (^{13}C) on a Bruker AS-200 or a Bruker DRX-200 instrument with the solvent signals used as reference. IR spectra were recorded with a Perkin-Elmer Spectrum 100 FT-IR spectrometer instrument from KBr pellets. Mass spectra were obtained with a JEOL JMS-700 or Finnigan TSQ 700/Bruker ApexQe hybrid 9.4 FT-ICR instrument. Electronic spectra were measured with a Tidas II J&M or a Jasco V-570 UV/vis/NIR-spectrophotometer. EPR measurements were preformed on a Bruker ELEXSYS-E-500 instrument at 125 K; spin-Hamiltonian parameters were obtained by simulation of the spectra with XSophe.[46] For electrochemical measurements a BAS-100B workstation was used, with a three-electrode setup, consisting of a glassy carbon working, a Pt-wire auxiliary, and, for MeCN solutions, an $Ag/AgNO_3$ reference electrode (0.01 M $AgNO_3$, 0.1 M $(Bu_4N)(PF_6)$, degassed CH_3CN), solutions of the complexes in MeCN/0.1 M $(Bu_4N)(PF_6)$; for H_2O solutions, an Ag/AgCl reference electrode (3 M NaCl, degassed and deionized H_2O), solutions of the complexes in H_2O, 0.1 M KNO_3; the potential of the Fc^+/Fc-couple for the MeCN setup had a value of +91 mV (MeCN, scan rate of 100 mV/s); the potential of the Fc^+/Fc-couple for the H_2O setup had a value of +195 mV, (H_2O, scan rate of 100 mV/s). Potentiometric titrations were performed on 20 mL of samples (0.1 M KCl for pK_a values, 0.2 M $NaClO_4$ for complex stabilities, 0.1 mol/L of the respective metal ion, 0.1 mol/L ligand) in various dioxane-water mixtures (50%, 55%, 60%),[47−50] T = 298 K; HCl was used to adjust the initial pH for pK_a titration, $HClO_4$ for complex stabilities; 0.1 mol/L KOH (CO_2-free, titration with potassium hydrogen phthalate); all solutions were kept under Ar. The measurements were done with a pH meter equipped with a 6.0202.100 combined electrode (Metrohm), a 665 Dosimat automatic buret (Metrohm). Data were fitted with Hyperquad.[51] Each titration was repeated at least twice. Cyclam was used as the competing ligand. Magnetic measurements were realized by magnetic balance (Alfa-Magnetic Susceptibility Balance, standard $Hg[Co(SCN)_4]$) or by SQID measurements (MPMS XL 5,Quantum-Design, RSO-mode). Elemental analyses were obtained from the analytical laboratories of the chemical institutes at the University of Heidelberg on a Vario EL (Elementar) instrument.

X-ray Crystal Structure Structure Determinations. Crystal data and details of the structure determinations are listed in the Supporting Information, Table S4. Intensity data were collected with a Bruker AXS Smart 1000 CCD diffractometer (Mo Kα radiation, graphite monochromator, l = 0.71073 Å). Data were corrected for air and detector absorption, Lorentz, and polarization effects;[52] absorption by the crystal was treated with a semiempirical multiscan method.[53,54]

The structures were solved by conventional direct methods[55,56] (ligands L^2 and $L^5 \cdot x$MeOH; complex $[Cu(L^4)][BF_4]_2 \cdot$NCMe), by the charge flip procedure[57−60] (complex $[Ni(L^4)][ClO_4]_2 \cdot xH_2O$) or by the heavy atom method combined with structure expansion by direct methods applied to difference structure factors (all others).[61,62] Refinement was carried out by full-matrix least-squares methods based on F^2 against all unique reflections.[63,64] All non-hydrogen atoms were given anisotropic displacement parameters.

The tetrafluoroborate and perchlorate anions were frequently found disordered. In such cases, split atom models were used and/or B−F and F···F (or Cl−O and O···O, respectively) distances were restrained to sensible values during refinement. Most of the crystals were found to contain solvent of crystallization, often with fractional population, namely, acetonitrile ($[M(L^2)NCMe][X]_2 \cdot$NCMe, M = Co, Cu, Zn; $[M(L^3)][X]_2 \cdot$NCMe, M = Cu, Ni; $[M(L^4)][X]_2 \cdot$NCMe, M = Co, Cu; $[Co(L^5)][X]_2 \cdot 3$ NCMe), water ($[M(L^4)][ClO_4]_2 \cdot xH_2O$, M = Ni ($x$ = 0.27), Zn (x = 0.28) or methanol ($[Ni(L^5)][X]_2 \cdot 1.25$ MeOH), $L^5 \cdot 0.2$ MeOH).

Hydrogen atoms were generally input at calculated positions and refined with a riding model. In the structures of the metal-free ligands the positions of most hydrogen atoms (except those of the methyl groups and the solvent methanol) were taken from difference Fourier syntheses and refined. Water in the structure of $[Ni(L^4)][ClO_4]_2 \cdot 0.27\ H_2O$ was refined as a rigid group. No hydrogens could be located for the solvent water molecule in $[Zn(L^4)][ClO_4]_2 \cdot 0.28\ H_2O$.

Computational Details. DFT calculations were performed with the software package Gaussian.[65] Full structural optimizations were done with B3LYP[66−68]/6-31G[69−78] d for all transition metal complexes. Frequency calculations were done on all optimized structures to verify their nature. Molecular mechanics calculations were done with the MOMEC program[79] and force field.[7,24,34,80]

(46) Hanson, G. R.; Gates, K. E.; Noble, C. J.; Griffin, M.; Mitchell, A.; Benson, S. *Inorg. Chem.* **2004**, *98*, 903.
(47) Gyenes, I. *Titration in nichtwässrigen Medien*; Enke Verlag: Stuttgart, **1970**.
(48) Yasuda, M. *Bull. Chem. Soc. Jpn.* **1959**, *32*, 429.
(49) Tencheva, J.; Velinov, G.; Budevsky, O. *Arzneim.-Forsch.* **1979**, *29*, 1331.
(50) Shedlovsky, T.; Kay, R. L. *J. Phys. Chem.* **1956**, *60*, 151.
(51) Gans, P.; Sabatini, A.; Vacca, A. *Talanta* **1996**, *43*, 1739.
(52) *SAINT*; Bruker AXS: Madison, WI, **2007**.
(53) Blessing, R. H. *Acta Crystallogr.* **1995**, *A51*, 33.
(54) Sheldrick, G. M. *SADABS*-2004/1 ed.; Bruker AXS: Madison, WI, **2004-2008**.
(55) Sheldrick, G. M. University of Göttingen: Göttingen, Germany, **1986**.
(56) Sheldrick, G. M. *Acta Crystallogr., Sect. A* **1990**, *46*, 467.
(57) Oszlànyi, G.; Suto, A. *Acta Crystallogr.* **2004**, *A60*, 134.
(58) Oszlànyi, G.; Suto, A. *Acta Crystallogr.* **2005**, *A61*, 147.
(59) Spek, A. L. Utrecht University, The Netherlands, **2003**.
(60) Spek, A. L. *J. Appl. Crystallogr.* **2003**, *36*, 7.
(61) Beurskens, P. T. In *Crystallographic Computing 3*; Sheldrick, G. M., Kruger, C., Goddard, R., Eds.; Clarendon Press: Oxford, U.K., **1985**, p. 216.
(62) Beurskens, P. T.; Beurskens, G.; de Gelder, R., Smits, J. M. M.; Garcia-Granda, S.; Gould, R. O. Radboud University: Nijmegen, The Netherlands, **2008**.
(63) Sheldrick, G. M. University of Göttingen: Göttingen, **1997**.
(64) Sheldrick, G. M. *Acta Crystallogr.* **2008**, *A64*, 112.
(65) Frisch, M. J.; Trucks, G. W.; Schlegel, H. B.; Scuseria, G. E.; Robb, M. A.; Cheeseman, J. R.; Montgomery, J. A., Jr.; Vreven, T.; Kudin, K. N.; Burant, J. C.; Millam, J. M.; Iyengar, S. S.; Tomasi, J.; Barone, V.; Mennucci, B.; Cossi, M.; Scalmani, G.; Rega, N.; Petersson, G. A.; Nakatsuji, H.; Hada, M.; Ehara, M.; Toyota, K.; Fukuda, R.; Hasegawa, J.; Ishida, M.; Nakajima, T.; Honda, Y.; Kitao, O.; Nakai, H.; Klene, M.; Li, X.; Knox, J. E.; Hratchian, H. P.; Cross, J. B.; Bakken, V.; Adamo, C.; Jaramillo, J.; Gomperts, R.; Stratmann, R. E.; Yazyev, O.; Austin, A. J.; Cammi, R.; Pomelli, C.; Ochterski, J. W.; Ayala, P. Y.; Morokuma, K.; Voth, G. A.; Salvador, P.; Dannenberg, J. J.; Zakrzewski, V. G.; Dapprich, S.; Daniels, A. D.; Strain, M. C.; Farkas, O.; Malick, D. K.; Rabuck, A. D.; Raghavachari, K.; Foresman, J. B.; Ortiz, J. V.; Cui, Q.; Baboul, A. G.; Clifford, S.; Cioslowski, J.; Stefanov, B. B.; Liu, G.; Liashenko, A.; Piskorz, P.; Komaromi, I.; Martin, R. L.; Fox, D. J.; Keith, T.; Al-Laham, M. A.; Peng, C. Y.; Nanayakkara, A.; Challacombe, M.; Gill, P. M. W.; Johnson, B.; Chen, W.; Wong, M. W.; Gonzalez, C.; Pople, J. A.; *Gaussian 03*; Gaussian, Inc.: Wallingford, CT, **2003**.
(66) Becke, A. D. *J. Chem. Phys.* **1992**, *96*, 2155.
(67) Becke, A. D. *J. Chem. Phys.* **1992**, *97*, 9713.
(68) Becke, A. D. *J. Chem. Phys. B* **1993**, *98*, 5648.
(69) Ditchfield, R.; Hehre, W. J.; Pople, J. A. *J. Chem. Phys.* **1971**, *54*, 724.
(70) Hehre, W. J.; Ditchfield, R.; Pople, J. A. *J. Chem. Phys.* **1972**, *56*, 2257.
(71) Hariharan, P. C.; Pople, J. A. *Mol. Phys.* **1974**, *27*, 209.
(72) Gordon, M. S. *Chem. Phys. Lett.* **1980**, *76*, 163.
(73) Hariharan, P. C.; Pople, J. A. *J. Chem. Phys.* **1973**, *82*, 213.
(74) Blaudeau, J.-P.; McGrath, M. P.; Curtiss, L. A.; Radom, L. *J. Chem. Phys.* **1997**, *107*, 5016.
(75) Francl, M. M.; Pietro, W. J.; Hehre, W. J.; Binkley, J. S.; DeFrees, D. J.; Pople, J. A.; Gordon, M. S. *J. Chem. Phys.* **1982**, *77*, 3654.
(76) Binning, R. C., Jr.; Curtiss, L. A. *J. Comp. Chem.* **1990**, *11*, 1206.
(77) Rassolov, V. A.; Pople, J. A.; Ratner, M. A.; Windus, T. L. *J. Chem. Phys.* **1998**, *109*, 1223.
(78) Rassolov, V. A.; Ratner, M. A.; Pople, J. A.; Redfern, P. C.; Curtiss, L. A. *J. Comp. Chem.* **2001**, *22*, 976.
(79) Comba, P.; Hambley, T. W.; Okon, N.; Lauer, G. *MOMEC97, a molecular modeling package for inorganic compounds*; Heidelberg, **1997**.
(80) Bol, J. E.; Buning, C.; Comba, P.; Reedijk, J.; Ströhle, M. *J. Comput. Chem.* **1998**, *19*, 512.

Syntheses. ***Caution!*** *Although no difficulties were found with the perchlorate salts described, these are potentially explosive and need to be handled with care. Heating, especially when dry, must be avoided.*

3-((Dimethylamino)methyl)-1,5-diphenyl-7-(1,4,6-trimethyl-1,4-diazepan-6-yl)-3,7-diazabicyclo[3.3.1]nonan-9-one (L^3). 2.5 mmol of N^1,N^1-dimethylethane-1,2-diamine, 5.1 mmol paraformaldehyde and 3 mL of glacial acetic acid were mixed at 0 °C in 5 mL of EtOH(abs) under Ar. Ice bath was removed and 2.5 mmol of 1-(1,4,6-trimethyl-1,4-diazacycloheptane-6-yl)-3,5-diphenylpiperidine-4-one in 4 mL of EtOH(abs) were added. The reaction mixture was stirred for 30 h at 70 °C. After complete removal of solvents, the resulting orange solid was suspended in diethyl ether. Basic KOH-solution was added, and the two phases were stirred until no insoluble solids were left. Organic phase was separated, and the aqueous phase extracted twice with diethyl ether. Combined organic phases were dried shortly with Na_2SO_4. Solvent was removed under reduced pressure yielding white foam in 1.8 mmol (72%) which was used without further purification. For titration experiments and analytical data the white foam was cleaned by column chromatography (silica, dioxane 8.4/Net_3 1.2/CH_3OH 0.4.) ^{1}H NMR ($CDCl_3$, 200.13 MHz) δ = 1.13 (s, 3H, CH_3); 2.22 (s, 6H, N-$(CH_3)_2$), 2.24 (m, 6H, N-CH_3); 2.24 (d, ^2J = 13.4 Hz, 2H, C-CH_{2ax}); 2.46 (m, 6H, CH_2-CH_2; $CH_2-N(CH_3)_2$); 2.65 (m, 2H, CH_2-$(CH_2-N(CH_3)_2)$); 2.78 (d, ^2J = 13.4 Hz, 2H, C-CH_{2eq}); 3.07 (d, ^2J = 10.6 Hz, 2H, CH_{2ax}-N-$(CH_2-CH_2-N-(CH_3)_2)$); 3.26 (d, ^2J = 11.2 Hz, 2H, N-CH_{2ax}-C); 3.48 (d, ^2J = 10.6 Hz, 2H, CH_{2eq}-N-$(CH_2-CH_2-N-(CH_3)_2)$); 3.77 (d, ^2J = 11.2 Hz, 2H, N-CH_{2eq}-C); 7.24 (m, 10H, CH_{Ph}). ^{13}C NMR ($CDCl_3$, 50.33 MHz) 25.13 (1C, CH_3); 47.53 (2C, N-$(CH_3)_2$); 48.08 (2C, CH_3); 53.57 (1C, CH_2-C-N$(CH_3)_2$); 54.98 (1C, C-CH_3); 55.13 (1C, $CH_2-N(CH_3)_2$); 58.97 (2C, C-CH_2-N); 60.02 (2C, C-C_{Ph}), 62.13 (2C, CH_2-CH_2); 64.92 (2C,N-CH_2-C); 65.93 (2C, CH_2-$(N-CH_2-CH_2-N(CH_3)_2)$); 126.67 (4C, $CH_{Ph/p}$); 127.12 (4C, $CH_{Ph/o}$); 127.58 (2C, $CH_{Ph/m}$); 143.00 (2C, C_{Ph}); 148.73. *IR* (KBr-pellet) 3409; 3051; 2937; 2803; 1717; 1599; 1458; 1367; 713; 696. FAB MS *m*/*z* 504.6 $[L^3H]^+$. Elemental analyses calcd: C: 73.92, H: 9.00, N: 13.90 found: C: 73.94, H: 8.88, N:12.87 .

1,5-Diphenyl-3-(2-picolylamine)-7-(1,4,6-trimethyl-1,-4-diazacycloheptane-6-yl)-diaza-bicyclo-[3.3.1]-nonane-9-none (L^4). 1.3 mmol of 2-picolylamine, 2.8 mmol formaldehyde solution, and 0.3 mL of glacial acetic acid were mixed at 0 °C in 6 mL of MeOH. Ice bath was removed and 1.3 mmol of 1-(1,4,6-trimethyl-1,4-diazacycloheptane-6-yl)-3,5-diphenylpiperidine-4-one in 4 mL of MeOH were added. The reaction mixture was stirred for 5 h at 65 °C. After complete removal of solvents, the resulting orange solid was suspended in diethyl ether. Basic KOH-solution was added, and the two phases were stirred until no insoluble solids are left. Organic phase was separated, and the aqueous phase extracted twice with diethyl ether. Combined organic phases were dried shortly with Na_2SO_4. Solvent was removed under reduced pressure yielding a white foam in 1.1 mmol (87%) which was used without further purification. ^{1}H NMR ($CDCl_3$, 200.13 MHz) δ = 1.19 (s, 3H, CH_3); 2.29 (m, 6H, N-CH_3); 2,31 (d, ^2J = 13.4 Hz, 2H, C-CH_{2ax}); 2.48 (m, 4H, CH_2-CH_2); 2.85 (d, ^2J = 13.4 Hz, 2H, C-CH_{2eq}); 3.20 (d, ^2J = 10.8 Hz, 2H, CH_{2ax}-N-CH_2-py); 3.28 (d, ^2J = 11.0 Hz, 2H, N-CH_{2ax}-C); 3.61 (d, ^2J = 10.8 Hz, 2H, CH_{2eq}-N-CH_2-py); 3.80 (d, ^2J = 11.0 Hz, 2H, N-CH_{2eq}-C); 3.89 (1H,CH_2-py); 3.92 (1H, CH_2-py); 7.26 (m, 10H,CH_{ph}); 7.67 (m, 3H, $CH_{3,4,5\text{-}py}$); 8.55 (m, 1H, $CH_{6\text{-}py}$). ^{13}C NMR ($CDCl_3$, 50.33 MHz) 25.90 (1C, CH_3); 48.54 (2C, CH_3); 54.39 (1C, C-CH_3); 58.87 (2C, C-CH_2-N); 59.85 (2C, C-C_{ph}), 61.79 (2C, CH_2-CH_2); 63.36 (1C, CH_2-py);64.92 (2C,N-CH_2-C); 65.83 (2C, CH_2-N-CH_2-py); 122.15 (1C, $C_{py/p}$); 123.01 (1C, $C_{py/o}$); 126.47 (4C, $CH_{Ph/p}$); 126.59 (4C, $CH_{Ph/o}$); 127.51 (2C, $CH_{Ph/m}$); 136.30 (1C, CH-$CH_{py/m}$); 142.96 (2C, C_{Ph}); 148.73 (1C, $NCH_{py/o}$); 167.77 (1C, C_{py}). IR (KBr-pellet) 3409; 3058; 2938; 2807; 1720; 1589; 1570; 1497; 1474; 1446; 1433; 1360; 759; 698. MALDI-TOF MS (nibeol) *m*/*z* 524.7 $[L^4H]^+$.

1,5-Diphenyl-3,7-(di[1,4,6-Trimethyl-1,4-diazacycloheptan-6-yl])-diaza-bicyclo-[3.3.1]-nonan-9-one (L^5). 10.2 mmol of 1,4,6-trimethyl-1,4-diazepan-6-amine, 20.5 mmol formaldehyde solution, and 1.6 mL of glacial acetic acid were mixed at 0 °C in 15 mL of THF. Ice bath was removed, and 5.0 mmol of 1,3-diphenylpropan-2-one in 5 mL of THF were added. The reaction mixture was stirred for 29 h at 65 °C. Stirring was continued for additional 24 h at rt. After complete removal of solvents, the resulting orange solid was dissolved in DCM and extracted with 5 × 200 mL 0.1 M HCl. The aqueous phase was made strongly alkaline by adding KOH and extracted with diethylether. The organic phase was dried shortly with Na_2SO_4. Solvent was removed under reduced pressure yielding white foam in 3.1 mmol (61%). Crystallization was realized by dissolving the solid in MeOH. The solution was left standing in a bulb covered by a drying tube filled with blue gel to avoid water diffusing into solution. For titration experiments and analytical data crystals were used. ^{1}H NMR ($CDCl_3$, 200.13 MHz) δ = 1.15 (s, 6H, CH_3); 2.20−2.25 (m, 16H, N-CH_3, N-CH_{2ax}); 2.35−2.57 (m, 8H, CH_2-CH_2); 2.82(d, ^2J = 12.6 Hz, 4H, N-CH_{2eq}); 2.85 (d, ^2J = 13.4 Hz, 2H, N-CH_{2ax}); 3.24 (d, ^2J = 11.0 Hz, 4H, N-CH_{2ax}-C); 3.75 (d, ^2J = 11.0 Hz, 4H, N-CH_{2eq}-C); 7.26 (m, 10H, -C_{Ph}). ^{13}C NMR ($CDCl_3$, 50.33 MHz) δ = 25.61 (2C, CH_3); 48.84 (4C, CH_3); 54.86 (2C, C-CH_3); 58.72 (4C, C-CH_2−N); 60.15 (4C, C−C_{Ph}), 62.11 (4C, CH_2-CH_2); 66.10 (4C,N-CH_2−C); 126.03 (2C, $CH_{Ph/p}$); 126.91 (4C, $CH_{Ph/o}$); 127.75 (4C, $CH_{Ph/m}$); 144.23 (2C, C_{Ph}); 212.50 (1C, CO). IR-(KBr-pellet) 3410; 3048; 3027; 2936 ; 2799; 1716; 1601; 1498; 1460; 1373; 717; 698. ESI$^+$MS (MeOH) *m*/*z* 605.6 [B3(CH_3OH)(H)]$^+$; 573.5 $[L^5H]^+$. Elemental analyses (L^5x0.2MeOH) calcd: C: 72.78, H: 9.16, N: 14.41; found: C: 72.63, H: 9.10, N: 14.21.

$[Co^{II}(L^2)](ClO_4)_2(NCCH_3)$. 0.35 mmol $Co^{II}(ClO_4)_2(H_2O)_6$ were dissolved in 2 mL of CH_3CN and added to a solution of 0.35 mmol L^2 in 2 mL of CH_3CN. After stirring at rt overnight, the solvent of the resulting violet solution was removed under reduced pressure. The solids have been dissolved in CH_3CN; diethylether diffusion resulted in a purple solid in 73% yield (0.25 mmol). IR (KBr-pellet): 3468; 2977; 2933; 1744; 1604; 1475; 1450; 1092; 769; 699. UV−vis (CH_3CN): λ_1 = 729 nm (ε = 20 L/(mol·cm)), λ_2 = 544 m (ε = 55 L/(mol·cm)), λ_3 = 525 nm (ε = 51 L/(mol·cm)), λ_4 = 494 nm (ε = 35 L/(mol·cm)), λ_5 = 426 nm (ε = 27 L/(mol·cm)). SQUID suggesting high-spin. ESI$^+$MS (CH_3CN) *m*/*z* 604.2 $[Co^{II}(L^2)ClO_4]^+$, 540.2 $[Co^{II}(L^2)Cl]^+$. Elemental analyses calcd: C: 48.86, H: 5.64, N: 10.68; found: C: 48.66, H: 5.55, N: 10.60.

$[Ni^{II}(L^2)](ClO_4)_2(NCCH_3)_2(H_2O)_3$. 0.38 mmol $Ni^{II}(ClO_4)_2(H_2O)_6$ were dissolved in 2.5 mL of CH_3CN and added to solution of 0.38 mmol L^2 in 2.5 mL of CH_3CN. After stirring at rt overnight, the resulting purple solution was treated with a diethyl ether diffusion resulting in violet crystals in 29% yield (0.11 mmol). IR (KBr-pellet): 3452; 3030; 2982; 2933; 1745; 1626; 1505; 1476; 1450; 1093; 757; 698. UV−vis (CH_3CN): λ_1 = 720 nm (ε = 7 L/(mol·cm)), λ_2 = 562 nm (ε = 30 L/(mol·cm)), λ_3 = 376 nm (ε = 27 L/(mol·cm)). SQUID suggesting high spin. ESI$^+$MS (CH_3CN) *m*/*z* 550.23 $[Ni^{II}(L^2)(HCOO)]^+$, 539.21 $[Ni^{II}(L^2)Cl]^+$. Elemental analyses calcd: C: 45.73, H: 6.00, N: 10.00; found: C: 45.64, H: 5.42, N: 9.93.

$[Zn^{II}(L^2)](ClO_4)_2(NCCH_3)_2(H_2O)_{1.5}$. 0.30 mmol $Zn^{II}(ClO_4)_2(H_2O)_6$ were dissolved in 5 mL of CH_3CN and added to solution of 0.3 mmol L^2 in 5 mL of CH_3CN. After stirring at rt overnight, the white precipitate was filtered off and rinsed with cold CH_3CN and CH_3OH to yield 19% (0.06 mmol) Crystals suitable for X-ray crystallography could be obtained by diethylether diffusion into CH_3CN solution of $Zn^{II}L^1$. IR (KBr-pellet): 3514; 2954; 1740; 1618; 1447; 1406; 1109; 702. ESI$^+$MS-(CH_3CN) *m*/*z* 555.2 $[Zn^{II}(L^2)(HCOO)]^+$, 545.2 $[Zn^{II}(L^2)Cl]^+$.

Elemental analyses calcd: C: 46.87, H: 5.78, N: 10.25; found: C: 46.68, H: 5.48, N: 10.04.

$[Co^{II}(L^3)](ClO_4)_2(CH_3CN)$. 0.29 mmol $Co^{II}(ClO_4)_2(H_2O)_6$ were dissolved in 2.5 mL of CH_3CN and added to solution of 0.29 mmol L^3 in 2.5 mL of CH_3CN. After stirring at rt overnight, the solvent of the resulting violet solution was removed under reduced pressure. The solids have been dissolved in CH_3CN; diethylether diffusion resulted in a purple solid in 67% yield (0.2 mmol). IR (KBr-pellet): 3446; 2989; 1735; 1605; 1487; 1450; 1096; 773; 703. UV−vis (CH_3CN): λ_1 = 749 nm (ε = 34 L/(mol·cm)), λ_2 = 565 m (ε = 141 L/(mol·cm)), λ_3 = 431 nm (ε = 101 L/(mol·cm)). SQUID suggesting high spin. ESI^+MS (CH_3CN) *m/z* 661.2 $[Co^{II}(L^3)ClO_4]^+$, 281.1 $[Co^{II}(L^3)]^{2+}$. Elemental analyses calcd: C: 49.38, H: 6.03, N: 10.47; found: C: 49.13, H: 6.01, N: 10.43.

$[Ni^{II}(L^3)](ClO_4)_2(NCCH_3)$. 0.20 mmol $Ni^{II}(ClO_4)_2(H_2O)_6$ were dissolved in 2.5 mL of CH_3CN and added to solution of 0.2 mmol L^3 in 2.5 mL of CH_3CN. After stirring at rt overnight, the resulting purple solution was treated with a diethyl ether diffusion resulting in blue crystals in 40% yield (0.08 mmol). IR (KBr-pellet): 3444; 3030; 2987; 2924; 1734; 1631; 1504; 1486; 1467; 1449; 1090; 770; 698. UV−vis (CH_3CN): λ_1 = 781 nm (ε = 36 L/(mol·cm)), λ_2 = 604 nm (ε = 40 L/(mol·cm)), λ_3 = 389 nm (ε = 110 L/(mol·cm)). SQUID suggesting high spin. ESI^+MS (CH_3CN) *m/z* 660.2 $[Ni^{II}(L^3)ClO_4]^+$, 280.6 $[Ni^{II}(L^3)]^{2+}$. Elemental analyses calcd: C: 49.40, H: 6.03, N: 10.47; found: C: 49.32, H: 6.01, N: 10.46.

$[Cu^{II}(L^3)](BF_4)_2](NCCH_3)$. 0.80 mmol $Cu^{II}(BF_4)_2(H_2O)_6$ were dissolved in 8 mL of CH_3CN and added to solution of 0.80 mmol L^3 in 8 mL of CH_3CN. After stirring at rt overnight, the resulting blue solution was treated with a diethyl ether diffusion resulting in blue crystals in 55% yield (0.44 mmol). IR (KBr-pellet): 3448; 3007; 2922; 1735; 1629; 1505; 1488; 1468; 1449; 1056; 70; 698. UV−vis (CH_3CN): λ_1 = 818 nm (ε = 149 L/(mol·cm)), λ_2 = 620 nm (ε = 464 L/(mol·cm)). EPR (CH_3CN:toluene, 1:1): $g_{\|}$ = 2.15 ($A_{\|}$ = 175 G); $g_{\perp}$ = 2.05 ($A_{\perp}$ = −30 G). *CV* ($E_{1/2}$, CH_3CN, 100 mV/s): −484 mV, ($E_{1/2}$, H_2O, *100 mV/s*): −368 mV. ESI^+MS (CH_3CN) *m/z* 585.3 $[Cu^{II}(L^3)(F)]^+$, 283.1 $[Cu^{II}(L^3)]^{2+}$. Elemental analyses calcd: C: 50.69, H: 6.19, N: 10.75; found: C: 50.61, H: 6.18, N: 10.71.

$[Zn^{II}(L^3)](ClO_4)_2(H_2O)(NCCH_3)$. 0.20 mmol $Zn^{II}(ClO_4)_2(H_2O)_6$ were dissolved in 5 mL of CH_3CN and added to solution of 0.2 mmol L^3 in 5 mL of CH_3CN. After stirring at rt overnight, the white precipitate was filtered off and rinsed with cold CH_3CN, CH_3OH, and H_2O to yield 25% (0.05 mmol). IR (KBr-pellet): 3617; 3545; 2992; 2937; 1736; 1603; 1477; 1466; 1117; 723; 700. $ESI^+MS(CH_3CN)$ *m/z* 666.2 $[Zn^{II}(L^2)ClO_4]^+$, 598.3 $[Zn^{II}(L^3)CH_3O]^+$, 283.6 $[Zn^{II}(L^3)]^{2+}$. Elemental analyses calcd: C: 47.92, H: 6.09, N: 10.16; found: C: 48.12, H: 5.85, N: 10.07.

$[Co^{II}(L^4)](ClO_4)_2(CH_3CN)$. 0.35 mmol $Co^{II}(ClO_4)_2(H_2O)_6$ were dissolved in 2.5 mL of CH_3CN and added to solution of 0.35 mmol L^4 in 2.5 mL of CH_3CN. After stirring at rt overnight, the solvent of the resulting violet solution was removed under reduced pressure. The solids have been dissolved in 50:50 H_2O/CH_3CN, diethyl ether diffusion resulted in purple crystals suitable for X-ray analysis in 20% yield (0.07 mmol). IR (KBr-pellet): 3422; 2977; 1738; 1611; 1487; 1448; 1090; 765; 701. UV−vis (CH_3CN): λ_1 = 559 nm (ε = 70 L/(mol·cm)), λ_2 = 538 nm (ε = 72 L/(mol·cm)), λ_3 = 425 nm (ε = 28 L/(mol·cm)). SQUID suggesting high spin. ESI^+MS (CH_3CN) *m/z* 681.2 $[Co^{II}(L^4)ClO_4]^+$, 291.1 $[Co^{II}(L^4)]^{2+}$. Elemental analyses calcd: C: 51.10, H: 5.39, N: 10.22 found: C: 51.09, H: 5.37, N: 10.25.

$[Ni^{II}(L^4)](ClO_4)_2(NCCH_3)$. 0.35 mmol $Ni^{II}(ClO_4)_2(H_2O)_6$ were dissolved in 2.5 mL of CH_3CN and added to solution of 0.35 mmol L^4 in 2.5 mL of CH_3CN. After stirring at rt overnight, the resulting purple solution was treated with a diethyl ether diffusion resulting in blue crystals in 26% yield (0.09 mmol). IR (KBr-pellet): 3446; 3052; 2975; 2923; 2860; 1733; 1615; 1501; 1488; 1448; 1091; 760; 699. UV−vis (CH_3CN): λ_1 = 732 nm (ε = 23 L/(mol·cm)), λ_2 = 551 nm (ε = 31 L/(mol·cm)). SQUID suggesting high spin. ESI^+MS (CH_3CN) *m/z* 680.2 $[Ni^{II}(L^4)ClO_4]^+$, 290.6 $[Ni^{II}(L^4)]^{2+}$. Elemental analyses calcd: C: 50.73, H: 5.29, N: 8.96; found: C: 50.92, H: 5.53, N: 9.09.

$[Cu^{II}(L^4)](BF_4)_2$. 0.12 mmol $Cu^{II}(BF_4)_2(H_2O)_6$ were dissolved in 5 mL of CH_3CN and added to a solution of 0.12 mmol L^4 in 5 mL of CH_3CN. After stirring at rt overnight, the resulting blue solution was treated with a diethyl ether diffusion resulting in blue crystals in 58% yield (0.07 mmol). IR (KBr-pellet): 3502; 3060; 2845; 1743; 1616; 1505; 1448; 1060; 765; 701. UV−vis (CH_3CN): λ_1 = 913 nm (ε = 198 L/(mol·cm)), λ_2 = 608 nm (ε = 280 L/(mol·cm)). EPR (CH_3CN:toluene, 1:1): $g_{\|}$ = 2.15 ($A_{\|}$ = 173 G); $g_{\perp}$ = 2.05 ($A_{\perp}$ = −30 G). *CV* ($E_{1/2}$, CH_3CN, 100 mV/s): −474 mV, ($E_{1/2}$, H_2O, *100 mV/s*): −295 mV. ESI^+MS (CH_3CN) *m/z* 293.4 $[Cu^{II}(L^4)]^{2+}$. Elemental analyses calcd: C: 50.89, H: 5.56, N: 8.99; found: C: 50.62, H: 5.53, N: 9.09.

$[Zn^{II}(L^4)](ClO_4)_2(H_2O)$. 0.35 mmol $Zn^{II}(ClO_4)_2(H_2O)_6$ were dissolved in 2.5 mL of MeOH and added to a solution of 0.35 mmol L^4 in 2.5 mL of MeOH. After stirring at rt overnight, the white precipitate was filtered off and rinsed with cold MeOH and H_2O to yield 38% (0.14 mmol). Crystals have been obtained from hot 50:50 MeOH/H_2O solution. IR (KBr-pellet): 3443; ; 3054; 2974; 2924; 2860; 1732; 1613; 1501; 1487; 1448; 1091; 759; 700. ESI^+MS (CH_3CN) *m/z* 686.2 $[Zn^{II}(L^4)ClO_4]^+$, 293.6 $[Zn^{II}(L^4)]^{2+}$. Elemental analyses calcd: C: 49.17, H: 5.38, N: 8.69; found: C: 48.98, H: 5.19, N: 8.54.

$[Co^{II}(L^5)](BF_4)_2$. 0.38 mmol $Co^{II}(BF_4)_2$ $(H_2O)_6$ were dissolved in 2 mL of CH_3CN and added to a solution of 0.35 mmol L^5 in 2 mL of CH_3CN. The reaction mixture was left stirring at rt overnight. The resulting pink solution was treated with a diethyl ether diffusion resulting in pink crystals in 71% yield (0.25 mmol). IR (KBr-pellet): 3435; 3028; 2976; 1742; 1630; 1481; 1447; 1057; 772; 703. UV−vis (CH_3CN): λ_1 = 864 nm (ε = 4 L/(mol·cm)), λ_2 = 567 nm (ε = 26 L/(mol·cm)), λ_3 = 471 nm (ε = 9 L/(mol·cm)). CV ($E_{1/2}$, CH_3CN, *100 mV/s*): +1504 mV. μ_{eff} = 4.73 μ_B ESI^+MS (CH_3CN) *m/z* 650.4 $[Co^{II}(L^5)F]^+$; 315.7 $[Co^{II}(L^5)]^{2+}$. Elemental analyses calcd: C: 52.20, H: 6.51, N: 10.43; found: C: 52.18, H: 6.74, N: 10.48.

$[Ni^{II}(L^5)](ClO_4)_2$. $[Ni^{II}(L^5)](ClO_4)_2$ has not been isolated and fully characterized. However, a crystal was obtained after approximately 2 weeks from stoichiometric amounts of Ni $(ClO_4)_2(H_2O)_6$ and L^5 dissolved in MeOH.

$[Cu^{II}(L^5)](BF_4)_2$. 0.34 mmol Cu^{II} $(BF_4)_2(H_2O)_6$ were dissolved in 5 mL of CH_3CN and added to a solution of 0.17 mmol L^5 in 5 mL of CH_3CN. The reaction mixture was heated for 1 min to reflux and left stirring at rt overnight. The resulting blue solution was treated with a diethyl ether diffusion resulting in blue crystals in 71% yield (0.12 mmol). IR (KBr-pellet): 3431; 3056; 2999; 2945; 2874; 2840; 1750; 1635; 1583; 1496; 1473; 1448; 1072; 770; 702. UV−vis (CH_3CN): λ_1 = 622 nm (ε = 382 L/(mol·cm)), λ_2 = 304 nm (ε = 6442 L/(mol·cm)). EPR (CH_3CN:toluene, 1:1): $g_{\|}$ = 2.18 ($A_{\|}$ = 165 G); $g_{\perp}$ = 2.02 ($A_{\perp}$ = −30 G). CV ($E_{1/2}$, CH_3CN, 100 mV/s): −440 mV, ($E_{1/2}$, H_2O, *100 mV/s*): −287 mV. $ESI^+MS(CH_3CN)$ *m/z* 317.9 $[Cu^{II}(L^5)]^{2+}$. Elemental analyses calcd: C: 51.90, H: 6.47, N: 10.38; found: C: 52.10, H: 6.44, N: 10.48.

$[Zn^{II}(L^5)](Cl)_2$ $ZnCl_2$. 0.62 mmol Zn^{II} $(Cl)_2$ were dissolved in 12 mL of CH_3CN and added to a solution of 0.52 mmol L^5 in 12 mL of CH_3CN. The reaction mixture was heated for 1 min to reflux and left stirring at rt overnight. The resulting white solid was filtered of and washed with CH_3CN. 45% yield (0.23 mmol). IR (KBr-pellet): 3461; 3058; 2971; 2950; 2926; 1740; 1637; 1479; 1446; 766; 696. ESI^+MS (CH_3CN) *m/z* 671.3 $[Zn^{II}(L^5)Cl]^+$, 318.2 $[Zn^{II}(L^5)]^{2+}$. Elemental analyses calcd: C: 49.13, H: 6.35, N: 10.84 found: C: 49.26, H: 6.24, N: 11.10.

Acknowledgment. Generous financial support by the German Science Foundation (DFG) and the University of Heidelberg (LGFG, "Molecular probes") is gratefully acknowledged.

Supporting Information Available: Sample titration curves, titration data of various solvent mixtures, a table with dd transition energies and intensities, electrochemical data, EPR spectra and their simulations, an extended table with structural data, including X-ray, DFT and MM in comparison, and the analysis of the trigonal distortion of the L^5-based complexes, and CIF files giving crystallographic data for all crystallographically characterized compounds. This material is available free of charge via the Internet at http://pubs.acs.org.